Structure-Preservation Model Aggregation for Two-Stage Inverters Based Large-Scale Photovoltaic System

Han, Yang; Lin, Xiangyang ; Yang, Ping; Xu, Lin; Xu, Yan; Blaabjerg, Frede

Published in:
IEEE Access

DOI (link to publication from Publisher):
10.1109/ACCESS.2019.2962303

Publication date:
2020

Document Version
Publisher's PDF, also known as Version of record

IEEE Access
Multidisciplinary | Rapid Review | Open Access Journal

Received December 3, 2019, accepted December 21, 2019, date of publication December 25, 2019, date of current version January 6, 2020.

Digital Object Identifier 10.1109/ACCESS.2019.2962303

Structure-Preservation Model Aggregation for Two-Stage Inverters Based Large-Scale Photovoltaic System

YANG HAN[1], (Senior Member, IEEE), XIANGYANG LIN[1], PING YANG[1], LIN XU[2], YAN XU[3], (Senior Member, IEEE), AND FREDE BLAABJERG[4], (Fellow, IEEE)

[1]School of Mechanical and Electrical Engineering, University of Electronic Science and Technology of China, Chengdu 611731, China
[2]Sichuan Electric Power Research Institute, Sichuan Electric Power Company, Chengdu 610072, China
[3]School of Electrical and Electronic Engineering, Nanyang Technological University, Singapore 639798
[4]Department of Energy Technology, Aalborg University, 9220 Aalborg, Denmark

Corresponding author: Yang Han (hanyang@uestc.edu.cn)

This work was supported in part by the National Natural Science Foundation of China under Grant 51977026, in part by the Natural Science Foundation of Guangdong Province under Grant 2018A030313494, and in part by the State Key Laboratory of Alternate Electrical Power System with Renewable Energy Sources under Grant LAPS18007.

ABSTRACT With the increasing penetration level of large-scale photovoltaic (PV) generator connected to the grid, an accurate simulation model is required for the dynamic analysis of the PV system. However, the detailed electromagnetic simulation of the large-scale system is complex and the dynamic response capability is estimated with obstacle caused by large computational burdens. Therefore, a precise dynamic aggregated model is indispensable for the displacement of the large-scale PV system. The structure-preservation based aggregated model with comprehensive equivalent parameters for large-scale PV system is proposed in this paper. A complete two-stage PV system model is established to analyze the dynamics of the system. Then, the aggregation method is obtained by comparing the dynamic equations of the detailed model with the aggregated model, which is based on the energy relationship in the PV system. Furthermore, four different case studies are considered including the aggregation of identical and different ten parallel-connected PV units both under the same irradiance condition, and the aggregation of different ten parallel-connected PV units under different irradiance and weak grid scenarios, where the aggregation models are obtained through the proposed equivalent modeling method. Finally, the effectiveness of the proposed aggregation method is verified by the simulation results from PSCAD/EMTDC platform, and the consistency between the aggregated model and the detailed model is confirmed under different disturbances of irradiance variation, and continuous symmetric and asymmetric grid faults.

INDEX TERMS Photovoltaic system, aggregation method, structure-preservation, equivalent parameters, model consistency.

I. INTRODUCTION

In power systems and micro-grid, the installed capacity of renewable energy power generation has increased a lot in past decades. Renewable energy is considered as a key factor in solving energy security due to the availability of photovoltaic (PV) resources, low cost and non-pollution on environment [1]. The existing research on photovoltaic (PV) power system mainly focuses on the mathematical modeling [2], [3] and the control strategies [4]–[6].

However, in the actual PV plant, the requirement of high-power level is generally satisfied through the cluster of multiple parallel PV units, which have the same structure and the same control method. Simulation analysis of multi-parallel system is implemented with the obstacle of the large time consumption and calculation space occupation. In addition, the dynamic characteristics of multi-parallel system in different operating environments are studied with difficulties because of a large-scale system. Therefore, the dynamic

The associate editor coordinating the review of this manuscript and approving it for publication was M. Jahangir.

aggregated model is necessary to simplify the analysis of large-scale system, which can ensure the characteristics stability of the system.

Model aggregation is a general method to obtain the equivalent system. Existing aggregation methods are mainly developed in inverter system [7]–[12] and the micro-grid system [13], [14]. Literatures [7]–[11] have proposed coherency criterion to group inverters with similar dynamic characteristic. In [7], the Hamilton-action principle has been applied into inverter system to derive the coherency criterion for the grid-connected inverter cluster, which can also be used in the order reduction of inverter-interfaced wind farms and PV systems, but equivalent parameters of are given directly without theoretical analysis. Similarly, coherency-based dynamic aggregation method using Hamilton-action for inverters is proposed in [8], and the applicability of the aggregated model for the stability analysis is verified by the simulation results both from frequency-domain and time-domain. A coherency equivalence criterion based on generalized differential for inverter system has been proposed in [9], but its coherency identification and parameters aggregation method are too difficult to measure. However, an equivalence method based on virtual synchronous generator (VSG) for multiple modular multilevel converters (MMC) has been established in [10], and the similarity of power angles characteristic between VSG-based MMC and synchronous generators was used to identify the coherent criterion. Furthermore, in [11], another coherency aggregation method with generalized eigenvalue perturbation technique for droop-controlled inverter networks has been investigated, and it shows the capability of accurately reproducing the system response after the clearance of the large disturbance.

Additionally, model aggregation and equivalence methods are preferred but not the coherency criterion in many literatures [12]–[14]. In [12], a reduced-order model of multi-parallel single-phase inverters has been obtained by model aggregation method, according to the relationship of state-variables between the accurate model and the aggregated model. The equivalent parameters are calculated under different real- and reactive-power setpoints in controller and different inverters in power ratings. However, this aggregated method is complex due to the solution of high-order matrix and it is not a simple aggregated method for other applications. A static equivalent model based on the grey-box theory of multi-microgrid was established in [13] through parameters optimization, but the dynamic characteristic cannot be reflected by this static model. In addition, the dynamic equivalent model for multi-microgrid has been proposed in [14], which is based on the structure preservation without time-consuming iterative calculations. The dynamic behaviors of a distributed energy source are studied by aggregating the external microgrids as an equivalent model, which includes the aggregation of buses, networks, drooped-controllers and power controllers. There are other methods like singular perturbation to establish the aggregation model of inverter [15], which can simplify the computational complexity of detailed models while maintaining the physical properties of the variables through fixing the slow variables as constant. In addition, it is worth noting that, although there are different equivalent methods, the same structure has been preserved in the aggregation model.

As for the large-scale PV system, the aggregation methods mainly focus on PV inverters on the ac-side, and the PV panels are considered as a constant voltage source. In [16], the calculation method for the aggregated parameters of multi-parallel PV system was proposed, but this method is only appropriate for establishing the equivalent model when the parameters are consistent with the operating environment. An equivalent method of PV plant in two different cases was considered in [17]. One is the group equivalence for the case of the interval of fault and post-fault recovery, the other is an independent equivalent method for the case without faults. In addition, an equivalent model of PV plant with virtual synchronous characteristic has been presented in [18]. This equivalent method is based on the synchronous power controller and the results contains the mechanical, electrical and droop equivalence. However, the structure of PV plant in [18] is not considering the PV panels. In [19], equivalent modeling of N-paralleled grid-connected inverters in the PV plant was analyzed, which considers the coupling problems caused by different grid impedances, but the PV arrays in PV inverters are also defined as constant dc source to simplify the analysis. Therefore, to sum up, a complete aggregation model for PV systems including the calculation of equivalent parameters should be evaluated.

The main contribution of this paper is the establishment of the comprehensive aggregation method for two-stage PV system, which contains the aggregated models of PV arrays, Boost converters, ac-side inverters and step-up transformers. In addition, it is worth noting that the comprehensive equivalent structure-preserving model is derived and the equivalent parameters are scaled by comparing the dynamic equations between the detailed model and the aggregated model, which is based on the energy relationship between two coherent PV systems. Different cases are studied, which includes two aggregation models of ten-parallel identical two-stage PV units and ten-parallel different PV units both under the same irradiance input condition, and two aggregation models of different PV units under diverse irradiance and weak grid scenarios. Two disturbances including irradiance variation, and continuous symmetrical and asymmetrical grid faults are separately applied in case studies to confirm the effectiveness of the aggregation method.

The rest of this paper is structured as follows: In Section II, detailed dynamic model of the two-stage PV system is established through differential equation in time-domain. In Section III, the energy relationship in two-stage PV system is provided to analyze the relationship of the state variables between two coherent PV systems, which is based on the Hamilton-action principle used in inverter system. Then, the equivalent parameter calculation method of the aggregated model is investigated through theoretical

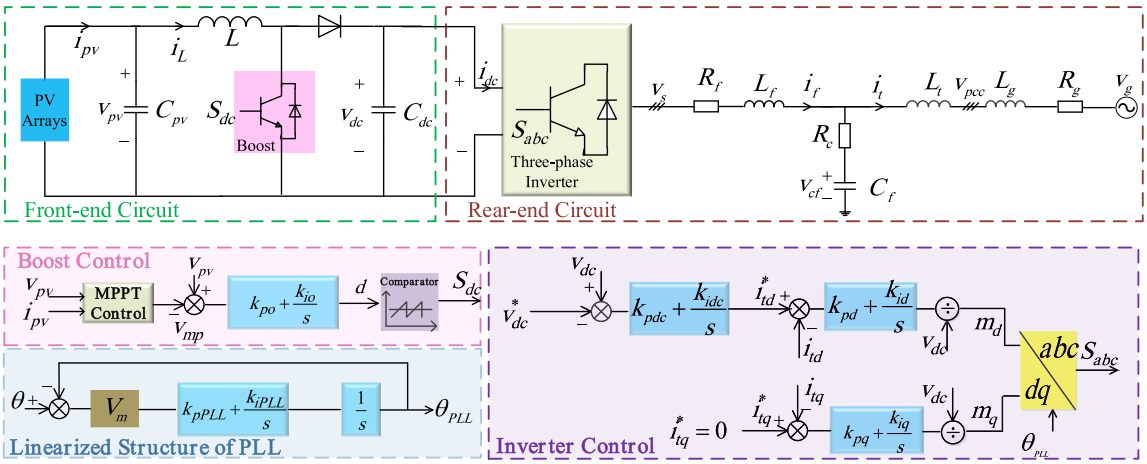

FIGURE 1. Simplified circuit and control strategy of the two-stage PV system.

derivations, which contains the equivalence of power-stage and control parameters. In Section IV, four cases are built in the PSCAD/EMTDC platform to verify the effectiveness of the aggregation model, and the consistency between the aggregated model and the detailed model is verified by the simulation results. Finally, the main conclusions are summarized in Section V.

II. MODELING OF THE TWO-STAGE PV SYSTEM

In order to identify the complete dynamics of the two-stage PV system, the modeling steps of each component are derived comprehensively. A simplified main circuit and the control strategy of two-stage PV system is shown in Fig. 1.

As shown in Fig. 1, C_{pv} is the smoothing capacitor of the front-end circuit, L is the energy storage inductor of the Boost circuit, and the capacitor of the dc-link is C_{dc}, v_s is the output voltage of three-phase inverter. L_f and C_f are the inductor and capacitor of the filter. R_f is the filter inductance parasitic resistance, and R_c is passive damping resistance. For the sake of avoiding the complicated calculation of parameters caused by different voltage levels, the parameters of the transformer and the grid are converted into the primary side. Therefore, L_t is the equivalent inductance of the transformer. L_g and R_g are the equivalent value of the grid inductance and resistance converted to the primary side of the transformer, and v_g is the grid voltage, which is converted to the primary side of transformer.

A. THE DYNAMICS OF FRONT-END CIRCUIT

Front-end circuit is composed of PV arrays and the Boost converter, and the detailed mathematical models of each component are introduced by the following parts.

According to [20], the mathematical model between output current i_{pv} and output voltage v_{pv} of the PV arrays is given by (1):

$$v_{pv} = \frac{N_s nkT}{q} \ln\left(\frac{N_p I_{sc} - i_{pv}}{N_p I_0} + 1\right) \tag{1}$$

in which, N_s and N_p are the number of PV cells connected in series and parallel, n is the ideally factor of diode, k is the Boltzmann's constant, T is the p-n junction temperature of the diode, q is the unit electric charge, I_{sc} is the short-circuit current of one PV cell at the conference temperature, and I_0 is the saturation current of the diode.

However, since the power generated by PV arrays is mainly determined by N_s and N_p, linearized model of PV arrays can be obtained as:

$$\begin{aligned} v_{pv} &= -\frac{N_s nkT}{q(N_p I_{sc} - I_{PV0} + N_p I_0)} i_{pv} = K_{pv} i_{pv} \\ K_{pv} &= -\frac{N_s nkT}{q(N_p I_{sc} - I_{pv0} + N_p I_0)} \end{aligned} \tag{2}$$

where I_{pv0} indicates the steady-state operating point of the PV array output current, and K_{pv} is a function of I_{pv0}.

The dynamics of the Boost converter is presented by the average model, and it is given by (3)-(5).

$$C_{pv}\frac{dv_{pv}}{dt} = i_{pv} - i_L \tag{3}$$

$$L\frac{di_L}{dt} = v_{pv} - (1-d)v_{dc} \tag{4}$$

$$C_{dc}\frac{dv_{dc}}{dt} = -i_{dc} + (1-d)i_L \tag{5}$$

where v_{dc} is the dc-link voltage, i_L is inductance current of the Boost circuit, and i_{dc} is the current flowing into the inverter, and d is the duty cycle of Boost converter and presented by (6)

$$d = (k_{po} + \frac{k_{io}}{s})(v_{mp} - v_{pv}) \tag{6}$$

where k_{po} and k_{io} are the proportional and integral gains of the PI controller in Boost circuit, and v_{mp} is the maximum voltage at the maximum power point obtained by the maximum power point tracking (MPPT) algorithm.

Supposing $\frac{dx_o}{dt} = k_{io}(v_{mp} - v_{pv})$, (6) can be rearranged into:

$$d = k_{po}(v_{mp} - v_{pv}) + x_o \tag{7}$$

where x_o is the dummy state variable.

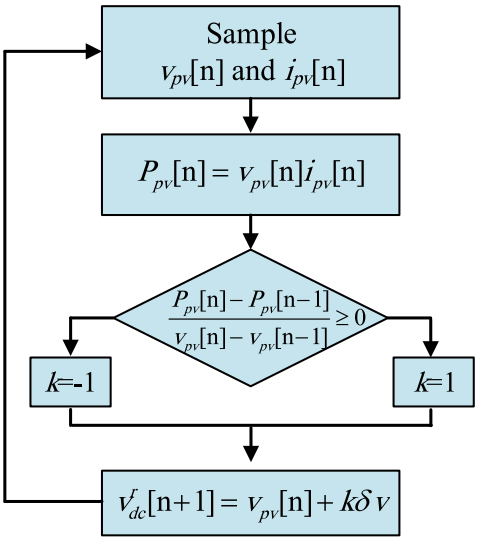

FIGURE 2. The flow chart of the basic P&O algorithm [23].

In general, the whole dynamics of the front-end circuit including controller are denoted as equations (2)-(5), and (7).

In this paper, P&O MPPT algorithm is used both for the aggregated model and the detailed model, which is evaluated in [21] and optimized in [22]. The flow chart of the basic P &O algorithm is shown in Fig. 2, where the δv is the voltage perturbation step [23]. The maximum power point can be reached by continuous imposing perturbation on the output voltage of PV arrays, where the perturbation direction is determined by comparing the output power with its value in last sample interval. Specifically, in every sample interval, if $dP_{pv}/dv_{pv} > 0$, the incremental perturbation will be imposed on the voltage. Then, when $dP_{pv}/dv_{pv} < 0$, the voltage will be regulated with decremental perturbation. The imposing perturbation will induce the fluctuation on output voltage in steady state. Therefore, the voltage perturbation step needs to be optimized to implement the balance between faster tracking speed and less fluctuation in steady state [24].

B. THE DYNAMICS OF REAR-END CIRCUIT

Adopting sinusoidal pulse-width modulation (PWM) and only considering the fundamental frequency, the dynamic models of the inverter in synchronous reference frame (SRF) are expressed as follows [25]:

$$i_{dc} = m_d i_{fd} + m_q i_{fq} \tag{8}$$

$$v_{sd} = \frac{1}{2} m_d v_{dc} \tag{9}$$

$$v_{sq} = \frac{1}{2} m_q v_{dc} \tag{10}$$

where m_d and m_q are the magnitude component of the modulation index in d-q frame, i_f and v_s represent the filter current and the inverter voltage component, respectively. Hence, i_{fd}, i_{fq}, v_{sd}, and v_{sq} are the corresponding components in d-q frame.

Since the transformer can be considered as the inductance, the filter can be regarded as an LCL filter. Similarly, the dynamic model of the filters in d-q frame is given by (11)-(16).

$$L_f \frac{di_{fd}}{dt} = \omega L_f i_{fq} + v_{sd} - v_{cfd} - R_c(i_{fd} - i_{td}) - R_f i_{fd} \tag{11}$$

$$L_f \frac{di_{fq}}{dt} = -\omega L_f i_{fd} + v_{sq} - v_{cfq} - R_c(i_{fq} - i_{tq}) - R_f i_{fq} \tag{12}$$

$$C_f \frac{dv_{cfd}}{dt} = \omega C_f v_{cfq} + i_{fd} - i_{td} \tag{13}$$

$$C_f \frac{dv_{cfq}}{dt} = -\omega C_f v_{cfd} + i_{fq} - i_{tq} \tag{14}$$

$$L_t \frac{di_{td}}{dt} = \omega L_t i_{tq} + R_c(i_{fd} - i_{td}) + v_{cfd} - v_{pccd} \tag{15}$$

$$L_t \frac{di_{tq}}{dt} = -\omega L_t i_{td} + R_c(i_{fq} - i_{tq}) + v_{cfq} - v_{pccq} \tag{16}$$

where i_t represents the current flowing through the equivalent inductance of transformer, v_{cf} is the voltage of filter capacitance, v_{pcc} is the voltage at the point of common coupling (PCC), and ω is fundamental angular frequency of grid.

In order to establish complete model of the two-stage PV system, the three-phase PLL is also considered, the linearized structure of the PLL is shown in Fig. 1. The dynamics of PLL can be derived as follows [26]:

$$\omega_{PLL} = k_{pPLL} v_q + k_{iPLL} \int v_q dt \tag{17}$$

$$\theta_{PLL} = \int \omega_{PLL} dt \tag{18}$$

where ω_{PLL} and θ_{PLL} represent angular frequency and coordinate transformation angle of PLL, and k_{pPLL} and k_{iPLL} are proportional and integral gains of the PI controller in PLL.

The ac-side inverter control is used to achieve a unity power factor, which consists of outer voltage control and inner current control in the synchronous reference frame, as shown in Fig. 1. The current reference i_{td}^* is determined by the PI controller in outer voltage loop, and the modulation index m_d and m_q are obtained through the PI current controller in SRF. Hence, the dynamics of the controller are presented as the follows.

$$i_{td}^* = k_{pdc}(v_{dc} - v_{dc}^*) + k_{idc} \int (v_{dc} - v_{dc}^*) dt \tag{19}$$

$$m_d = \frac{1}{v_{dc}} [k_{pd}(i_d^* - i_d) + k_{id} \int (i_d^* - i_d) dt] \tag{20}$$

$$m_q = \frac{1}{v_{dc}} [k_{pq}(i_q^* - i_q) + k_{iq} \int (i_q^* - i_q) dt] \tag{21}$$

where i_{td}^* is the current reference in d-axis, k_{pdc} and k_{idc} represent the proportional and integral gains of the PI controller in the outer voltage loop. Similarly, k_{pd}, k_{id}, k_{pq} and k_{iq} are proportional and integral gains of PI current controller in d-axis and q-axis, respectively.

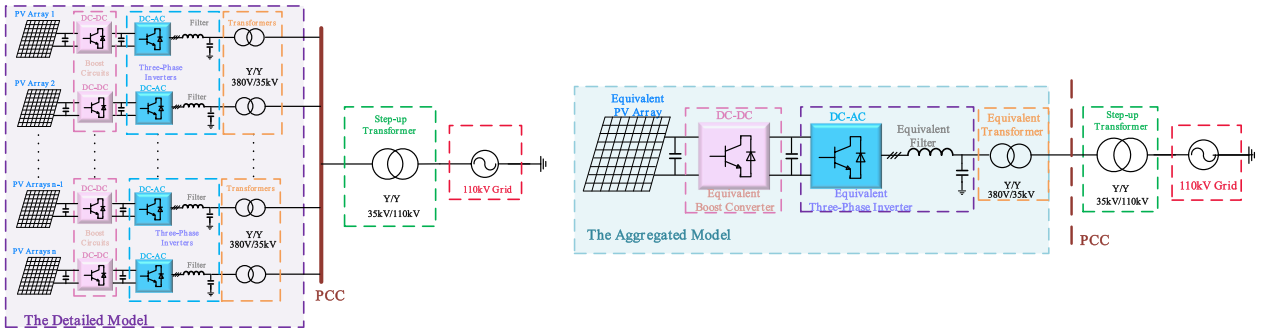

FIGURE 3. The schematic diagram of the detailed model and the aggregated model. (a). the detailed model; (b). the aggregated model.

Assuming $\frac{dx_{dc}}{dt} = k_{idc}(v_{dc} - v^*_{dc})$, $\frac{dx_d}{dt} = k_{id}(i^*_{td} - i_{td})$, and $\frac{dx_q}{dt} = k_{iq}(i^*_{tq} - i_{tq})$. Hence, (22)-(24) can be obtained:

$$i^*_{td} = k_{pdc}(v_{dc} - v^*_{dc}) + x_{dc} \tag{22}$$

$$v_{dc}m_d = k_{pd}(i^*_{td} - i_{td}) + x_d \tag{23}$$

$$v_{dc}m_q = k_{pq}(i^*_{tq} - i_{tq}) + x_q \tag{24}$$

where x_{dc}, x_d and x_q are the dummy state variables and v^*_{dc} represents the reference signal of dc-link voltage.

In general, the complete dynamics of rear-end inverter including controller and PLL are denoted as equations (8)-(18), (22)-(24).

III. AGGREGATION METHOD FOR TWO-STAGE PV SYSTEM

In this section, the comprehensive calculation methods of aggregated parameters are proposed by comparing the dynamic equations of the detailed model with the aggregated model, which is based on the proportional relationship of state-variables between two coherent PV systems and the capacity weighting method. The proposed aggregation method is aimed to provide an equivalent parameter calculation method for the multi-parallel PV units, which are coherent and satisfy the coherency criterion in [7], [8]. Specifically, the coherent condition for PV system is that the maximum variation ratio of the grid-connected line currents of different PV units during a disturbance (symmetric or asymmetric grid fault) is less than the coherency tolerance ε. In addition, it is worth noting that the coherent condition is satisfied between multi-parallel PV units of the detailed model in this paper.

The framework of the detailed model and aggregated model are shown in Fig. 3. The aggregation of PV arrays, Boost converters, three-phase inverters, filters and transformers are included to implement a complete equivalent model, which is introduced in detail in the following part.

Fig. 3 demonstrates that both the detailed model and the aggregated model are connected to the 110 kV grid with a step-up transformer through PCC. In addition, the multi-parallel PV units and the equivalent PV system are tied to PCC through a Y/Y transformer with the voltage level of 380 V/35 kV, where the aggregation model of this transformer is evaluated in this paper.

A. ENERGY RELATIONSHIP IN TWO-STAGE PV SYSTEM

Two coherent systems have the characteristic that all state-variables are proportional. According to the principle of Hamilton's Action analyzed in [7], [8], the sufficient and necessary condition for the proportion of the state variables is that the energy relationship of the system is proportional. In reverse, if the energy relationship is identified, the relationship of state-variables is obtained. Therefore, the Hamilton' action is extended to two-stage PV system to identify the energy relationship and further obtain the proportional relationship of state-variables between two coherent PV system. According to the analysis in [7], it can be easily concluded that the energy in PV system is composed of the magnetic field energy, the electric field energy and the generalized potential energy. The magnetic field energy consists of the energy storage in the inductor, and the electric field energy is composed of the energy storage in the capacitor. Since there exists energy exchange from dc-side to ac-side, and the energy dissipated by the resistor in PV system, the two-stage PV system is a non-conservative system [7], [8]. Hence, the generalized potential energy U in two-stage PV system is defined as the integral of the sum of dc input power, ac output power and the power consumed by the resistance R_c and R_f to evaluate those energy of non-conservative system.

From the above analysis, it can be inferred that the proportional relationship of energy is satisfied between two coherent PV system. Furthermore, with the energy conservation law, it is equal to the proportion of magnetic field energy, and the proportion of the sum of electric field energy and the generalized potential energy. Hence, the energy relationship between two coherent PV systems is identified, which is given in (25) as shown at the bottom of the next page. where T is magnetic field energy, V is electric field energy, and U is the generalized potential energy in two-stage PV system [7], and k is a constant value. The subscript 1, and 2 are used to distinguish arbitrary two coherent PV system.

From (25), the following relationship of state variables can be obtained:

$$\begin{cases} \dfrac{R_{f1}}{R_{f2}} = \dfrac{R_{c1}}{R_{c2}} = \dfrac{L_1}{L_2} = \dfrac{L_{f1}}{L_{f2}} = \dfrac{L_{t1}}{L_{t2}} = \dfrac{C_{pv2}}{C_{pv1}} \\ = \dfrac{C_{dc2}}{C_{dc1}} = \dfrac{C_{f2}}{C_{f1}} = k_L \\ \dfrac{i_{L1}}{i_{L2}} = \dfrac{i_{f1}}{i_{f2}} = \dfrac{i_{t1}}{i_{t2}} = \dfrac{i_{pv1}}{i_{pv2}} = \sqrt{\dfrac{k}{k_L}} \\ \dfrac{v_{pcc1}}{v_{pcc2}} = \dfrac{v_{dc1}}{v_{dc2}} = \dfrac{v_{cf1}}{v_{cf2}} = \dfrac{v_{pv1}}{v_{pv2}} = \sqrt{kk_L} \end{cases} \tag{26}$$

where k_L is another constant value.

Based on the previous analysis, it is concluded that the relation in (26) is satisfied between state variables of arbitrary parallel units in the detailed model since they are coherent units. Furthermore, the model coherency remains unchanged after aggregation. Hence, the same proportional relationship can be found between the aggregated model and the detailed model.

B. PARAMETERS AGGREGATION METHOD FOR TWO-STAGE PV SYSTEM

1) AGGREGATION MODEL OF PV ARRAYS

Since the aggregated model needs satisfy the same power level with the detailed model, capacity weighting method [16] can be used to the aggregation of PV arrays, and the total output power of the equivalent PV array should be equal to the sum of the output power of all PV arrays. Hence the output power of the equivalent PV arrays is given as:

$$S_{pveq} = \sum_{l=1}^{n} S_{pvl} \tag{27}$$

where S_{pveq} is the output power of the equivalent PV array and S_{pvl} represents the output power of l-th PV array in the detailed model. l varies from 1 to n, and n is the number of parallel PV unit in the detailed model.

As shown in Fig. 3, since the detailed model and the aggregated model are connected to the 110 kV grid with the same step-up transformer through PCC, it can be obtained that $v_{pccl} = v_{pcceq}$. Furthermore, with the third relationship in (26), there is:

$$v_{pveq} = v_{pvl} \tag{28}$$

In order to satisfy the power relationship in (27), the current of the aggregated PV array should be the sum of the currents of parallel PV units in the detailed model. In addition, the output voltage of PV arrays is mainly determined by N_s and the current is depended on the parallel number N_p.

Therefore, the calculating method of the aggregated PV arrays is given by (29).

$$N_{seq} = N_{sl}, \quad N_{peq} = \sum_{l=1}^{n} N_{pl} \tag{29}$$

in which N_{seq} is the series number of equivalent photovoltaic arrays and N_{peq} is the parallel number.

From (27)-(29), it is suggested that the output power of aggregated model is achieved by adding the parallel number of PV cells, and coherent units have the same PV voltage.

2) MPPT ALGORITHM IN THE AGGREGATED MODEL

It is worth noting that with certain irradiance and temperature condition, the power-voltage characteristic curve of PV array has a global peak value, which is corresponding to an optimum value of PV array voltage. If the voltage of PV array is regulated at the optimum value, the maximum power of PV array can be well tracked. In addition, the tracking speed and accuracy of P&O algorithm is determined by the sample interval and voltage perturbation step.

According to the aggregated method for the PV arrays, the PV output voltage of the aggregated model is the same with the PV voltages of multi-parallel units in the detailed model. It implies that the power-voltage characteristic curve of PV arrays in the aggregated model has minor difference with the detailed model. Therefore, it can be deduced that the maximum power of the aggregated model can be well tracked by adopting the same sample interval and perturbation step in MPPT algorithm with that in the detailed model.

3) AGGREGATION MODEL OF POWER-STAGE PARAMETERS

The circuit equation of each PV unit and the aggregated model can be obtained by rewriting the equations (3)-(5), (11)-(16) in section II, and they can be expressed as follows

$$\begin{cases} C_{pvl}\dfrac{dv_{pvl}}{dt} = i_{Ll} - i_{pvl} \\ \dfrac{1}{L_l}v_{pvl} - \dfrac{1-d_l}{L_l}v_{dcl} = \dfrac{di_{Ll}}{dt} \\ C_{dcl}\dfrac{dv_{dcl}}{dt} = (1-d_l)i_{Ll} - i_{dcl} \\ \dfrac{s_{abcl}}{L_{fl}}v_{dc} - \dfrac{1}{L_{fl}}v_{cfl} = \dfrac{di_{fl}}{dt} + \dfrac{R_{cl}+R_{fl}}{L_{fl}}i_{fl} \\ -\dfrac{R_{cl}}{L_{fl}}i_{tl} \\ C_{fl}\dfrac{dv_{cfl}}{dt} = i_{fl} - i_{tl} \\ \dfrac{1}{L_{tl}}v_{cfl} - \dfrac{1}{L_{tl}}v_{pccl} = \dfrac{di_{tl}}{dt} - \dfrac{R_{cl}}{L_{tl}}(i_{fl} - i_{tl}) \end{cases} \tag{30}$$

$$\begin{cases} \dfrac{T_1}{T_2} = \dfrac{L_1 i_{L1}^2 + L_{f1} i_{f1}^2 + L_{t1} i_{t1}^2}{L_2 i_{L2}^2 + L_{f2} i_{f2}^2 + L_{t1} i_{t2}^2} = k \\ \dfrac{V_1 + U_1}{V_2 + U_2} = \dfrac{C_{pv1}v_{pv1}^2 + C_{dc1}v_{dc1}^2 + C_{f1}v_{cf1}^2 + \int [i_{pv1}v_{pv1} + R_{f1}i_{f1}^2 + R_{c1}(i_{f1} - i_{t1})^2 + v_{pcc1}i_{t1}]dt}{C_{pv2}v_{pv2}^2 + C_{dc2}v_{dc2}^2 + C_{f2}v_{cf2}^2 + \int [i_{pv2}v_{pv2} + R_{f2}i_{f2}^2 + R_{c2}(i_{f2} - i_{t2})^2 + v_{pcc2}i_{t2}]dt} = k \end{cases} \tag{25}$$

$$\begin{cases} C_{pveq}\dfrac{dv_{pveq}}{dt} = i_{Leq} - i_{pveq} \\ \dfrac{1}{L_{eq}}v_{pvi} - \dfrac{1-d_{eq}}{L_{eq}}v_{dceq} = \dfrac{di_{Leq}}{dt} \\ C_{dceq}\dfrac{dv_{dceq}}{dt} = (1-d_{eq})i_{Leq} - i_{dceq} \\ \dfrac{s_{abceq}}{L_{feq}}v_{dceq} - \dfrac{1}{L_{feq}}v_{cfeq} = \dfrac{di_{feq}}{dt} \\ +\dfrac{R_{ceq}+R_{feq}}{L_{feq}}i_{feq} - \dfrac{R_{ceq}}{L_{feq}}i_{teq} \\ C_{feq}\dfrac{dv_{cfeq}}{dt} = i_{feq} - i_{teq} \\ \dfrac{1}{L_{teq}}v_{cfeq} - \dfrac{1}{L_{teq}}v_{pcceq} = \dfrac{di_{teq}}{dt} - \dfrac{R_{ceq}}{L_{teq}}(i_{feq} - i_{teq}) \end{cases} \tag{31}$$

where the subscript eq indicates the circuit equivalent parameters of the aggregated model, and s_{abc} is the switching function of the inverter. Superimposing the state equation of each parallel unit, (32) can be obtained:

$$\begin{cases} (\sum_{l}^{n} C_{pvl})\dfrac{dv_{pv}}{dt} = \sum_{l}^{n} i_{Ll} - \sum_{l}^{n} i_{pvl} \\ (\sum_{l}^{n} \dfrac{1}{L_l})v_{pv} - (\sum_{i}^{n} \dfrac{1}{L_l})(1-d_l)u_{dcl} = \sum_{l}^{n} \dfrac{di_{Ll}}{dt} \\ (\sum_{l}^{n} C_{dcl})\dfrac{dv_{dc}}{dt} = (1-d_l)\sum_{l}^{n} i_{Ll} - \sum_{l}^{n} i_{dcl} \\ (\sum_{l}^{n} \dfrac{1}{L_{fl}})s_{abcl}v_{dc} - \sum_{l}^{n} \dfrac{1}{L_{fl}}v_{cf} = \sum_{l}^{n} \dfrac{di_{fi}}{dt} \\ +\sum_{l}^{n} \dfrac{R_{cl}+R_{fl}}{L_{fl}}i_{fl} - \sum_{l}^{n} \dfrac{R_{cl}}{L_{fl}}i_{tl} \\ (\sum_{l}^{n} C_{fl})\dfrac{dv_{cf}}{dt} = \sum_{l}^{n} i_{fl} - \sum_{l}^{n} i_{tl} \\ (\sum_{l}^{n} \dfrac{1}{L_{tl}})v_{cf} - (\sum_{l}^{n} \dfrac{1}{L_{tl}})v_{pccl} = \sum_{l}^{n} \dfrac{di_{tl}}{dt} \\ -\sum_{l}^{n} \dfrac{R_{cl}}{L_{tl}}(i_{fl} - i_{tl}) \end{cases} \tag{32}$$

Ignoring the differences between PWM control of each PV unit and supposing each PV unit uses the same frequency triangular wave as the carrier, with the same voltage level of the grid and PCC, there is $s_{abcl} = s_{abceq}$. Hence, applying the third relationship in (26), it can be further obtained that $v_{dcl} = v_{dceq}$, $v_{cfl} = v_{cfeq}$. Moreover, supposing that the triangular carrier waves of front-end circuit use the same frequency, we get $d_l = d_{eq}$. Due to the power is the constant after aggregation, it is rational to consider that the equivalent current is the sum of the parallel units. Consequently, comparing the left side of (32) with (31), there is:

$$\begin{cases} C_{pveq} = \sum_{l}^{n} C_{pvl}, \quad C_{dceq} = \sum_{l}^{n} C_{dcl}, \; C_{feq} = \sum_{l}^{n} C_{fl} \\ \dfrac{1}{L_{eq}} = \sum_{l}^{n} \dfrac{1}{L_l}, \quad \dfrac{1}{L_{feq}} = \sum_{l}^{n} \dfrac{1}{L_{fl}}, \; \dfrac{1}{L_{teq}} = \sum_{l}^{n} \dfrac{1}{L_{tl}} \end{cases} \tag{33}$$

At the same time, with the constraint relationship in (26) and the equivalent equations in (33), the relationship of the resistances can be obtained by comparing the right side of (32) and (31), which is written as (34).

$$\frac{1}{R_{feq}} = \sum_{l}^{n} \frac{1}{R_{fl}}, \quad \frac{1}{R_{ceq}} = \sum_{l}^{n} \frac{1}{R_{cl}} \tag{34}$$

To sum up, (33) and (34) are the aggregation method for calculating the equivalent power-stage parameters of two-stage PV system.

4) AGGREGATION MODEL OF TRANSFORMER

According to (33), the reciprocal of impedance of the equivalent transformer is the sum of the reciprocal of impedances of the parallel transformers in PV units. The equivalent impedance will decrease after aggregation. Therefore, in order to keep the constant of primary side voltage level, the equivalent transformer capacity should increase, a simplified method is considered that the sum of the transformer capacities of each unit as the equivalent capacity, that is:

$$S_{teq} = \sum_{l}^{n} S_{tl} \tag{35}$$

where S_{teq} is the capacity of equivalent transformer.

It can be concluded from (35) that the capacity relationship between transformers corresponds to the power relationship between the aggregated model and the detailed model.

5) AGGREGATION MODEL OF CONTROL PARAMETERS

The two-stage PV system contains the front-end circuit control and inverter control, and the dynamics of equivalent Boost control in the aggregated model can be presented as:

$$d_{eq} = k_{poeq}(v_{mpeq} - v_{pveq}) + x_{oeq} \tag{36}$$

where d_{eq} represents the equivalent duty cycle of the Boost converter, x_{oeq} is the equivalent dummy state-variable, and v_{mpeq} denotes the maximum voltage at maximum power point of the equivalent PV arrays.

From the above analysis, it demonstrates that the output voltages of the PV arrays are the same, and the duty cycle of the Boost converter is identical. Moreover, with the same sample interval and perturbation step in P&O MPPT algorithm, the maximum voltage v_{mp} tracked by the MPPT algorithmic can be approximately seen as the same. Hence, comparing (7) and (36), we get:

$$k_{poeq} = k_{pol}, \quad k_{ioeq} = k_{iol} \tag{37}$$

where k_{poeq} and k_{ioeq} are the equivalent proportional and integral gains of the PI controller in the Boost converter, respectively.

The outer voltage loop of inverter is used to maintain the dc-link voltage and generate the current reference in the d-axis. Since the dc-link voltage and the reference voltage is the same in both parallel PV units and the aggregated PV

system, the dynamic equation of the outer voltage loop of the equivalent model can be rewritten as:

$$i^*_{td\mathrm{eq}} = k_{pdceq}(v_{dceq} - v^*_{dceq}) + x_{dceq} = k_{pdceq}(v_{dc} - v^*_{dc}) + x_{dceq} \tag{38}$$

where i^*_{tdeq} is the equivalent current reference signal of d-axis, and x_{dceq} represents the equivalent state-variable of the aggregated model.

The current reference in the d-axis reflect the active power reference, and the power relationship between parallel PV units and equivalent system is $P_{eq} = \sum_{l=1}^{n} P_l$. Therefore, when the current reference can be well tracked, it is rational to deem that:

$$i^*_{tdeq} = \sum_{l=1}^{n} i^*_{tdl} \tag{39}$$

where i^*_{tdl} represents the current reference of the l-th PV unit.

The summation of equations of each PV unit can be presented as:

$$\sum_{l=1}^{n} i^*_{tdl} = \sum_{l=1}^{n} k_{pdcl}(v_{dc} - v^*_{dc}) + \sum_{l=1}^{n} x_{dcl} \tag{40}$$

Comparing (40) with (22) and combining (39), the equivalent control parameter of outer voltage loop can be obtained:

$$k_{pdceq} = \sum_{l=1}^{n} k_{pl}, \quad k_{idceq} = \sum_{l=1}^{n} k_{il} \tag{41}$$

where k_{pdceq} and k_{idceq} represent the equivalent proportional and integral gains of PI controller of outer voltage loop in inverter, respectively.

Since the inner current control loop is employed to generate the required active and reactive power, a power weighting factor Υ_l is introduced as:

$$\gamma_l = \frac{P_l}{P_{sum}} = \frac{P_l}{\sum_{l=1}^{n} P_l} \tag{42}$$

Therefore, the equivalent current control parameters in the d-q axis can be calculated by the power-scaling method, which is given as:

$$k_{pdeq} = \sum_{l=1}^{n} \gamma_l k_{pdl}, \quad k_{ideq} = \sum_{l=1}^{n} \gamma_l k_{idl} \tag{43}$$

$$k_{pqeq} = \sum_{l=1}^{n} \gamma_l k_{pql}, \quad k_{iqeq} = \sum_{l=1}^{n} \gamma_l k_{iql} \tag{44}$$

where k_{pdeq}, k_{ideq}, k_{pqeq}, and k_{iqeq} are the equivalent proportional and integral gains of PI controller of the inner current loop in d-axis and q-axis, respectively.

Generally, equations (37), (41), (43) and (44) denote the calculation method of the control parameters for the aggregated model.

IV. CASE STUDY AND SIMULATION VERIFICATION

Four case studies are implemented in this section to verify the effectiveness of the proposed aggregation method, which include:

Case 1: The aggregation model of ten-parallel identical PV units with the same irradiance input.

Case 2: The aggregation model of ten-parallel different PV units with the same irradiance input.

Case 3: The aggregation model of ten-parallel different PV units with the diverse irradiance input.

Case 4: The aggregation model of ten-parallel different PV units under weak grid condition.

In addition, two different disturbances including irradiance variation and grid faults are separately applied in those case studies to confirm the consistency between the aggregated model and the detailed model, which are introduced in detail in the following part.

A. DESCRIPTION OF THE SIMULATION SETTINGS

The detailed multi-parallel PV system and the aggregated PV system are both built in the platform of PSCAD/EMTDC version 4.5, and the equivalent parameters of the aggregated model are scaled by the theoretical analysis in Section III. The simulation time for both the aggregated model and the detailed model is set as 3 s with the same time step of 10 μs. In addition, all the simulations are conducted on the laptop with Intel(R) Core(TM) i5-4200M 2.50GHz CPU, and 8GB of RAM.

In PSCAD/EMTDC simulation platform, the whole block diagram of detailed PV system is shown in Fig. 4, where each parallel PV unit adopts the same control strategy and structure. Moreover, with structure-preservation method, the same power-stage structure and control method are applied in the aggregated model.

As shown in Fig. 4, the maximum power point operation of the PV arrays is realized by the Boost circuit control, the dual-loop control in double synchronous reference frame is utilized for rear-end inverter, and the discharging circuit adopting a separate dc voltage loop is added at the dc-link. The normal operation for the two-stage PV system under both symmetric and asymmetric grid fault can be achieved by this control scheme since the overcurrent caused by unbalanced grid fault can be eliminated by the negative sequence current controller, and the excess active power during fault operation can be consumed by the discharging circuit. The detailed description about this control scheme can be found in [27].

Irradiance variation is selected as one disturbance to verify the effectiveness of the aggregated model, which is applied in Case 1 and Case 2. The irradiance variation curve is shown in Fig. 5.

In addition, symmetrical and asymmetrical grid faults are selected as the other disturbance, which are applied in all Cases. The three-phase symmetric grid fault and single-phase to ground grid fault occur at $t = 1$ s and $t = 2$ s, respectively. The duration time of the grid faults is 0.5 s. Furthermore,

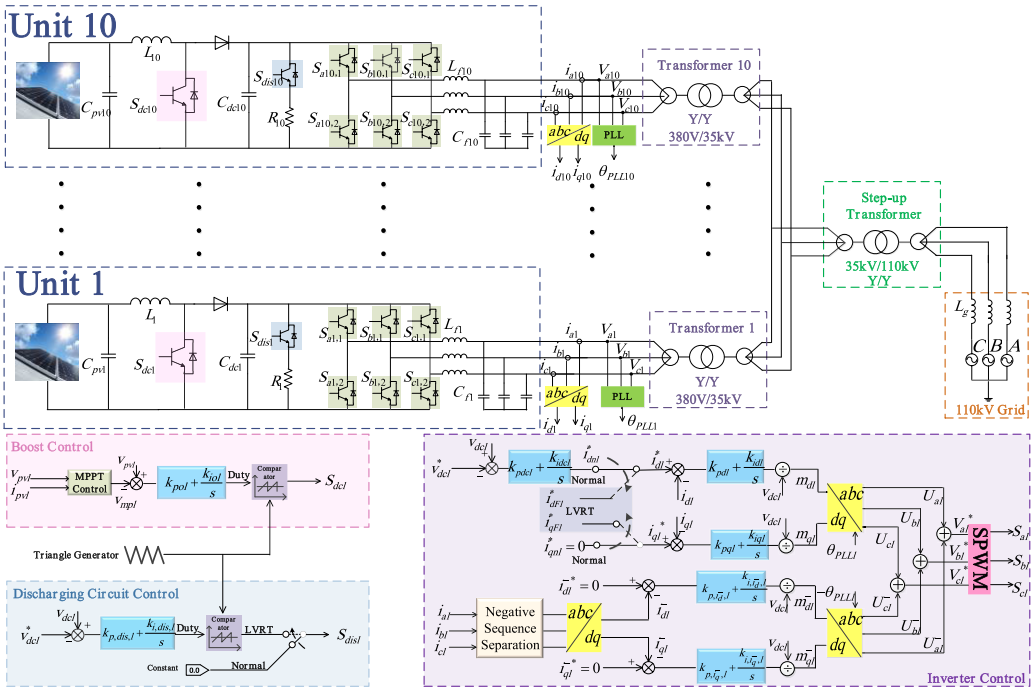

FIGURE 4. Overall block diagram of detailed multi-parallel two-stage PV system.

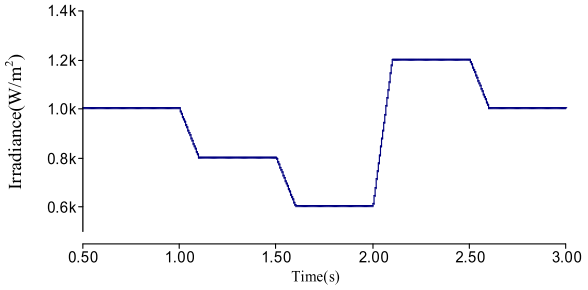

FIGURE 5. Irradiance variation curve in the case studies.

the compensating reactive and active power during the grid faults satisfies the criterion of low-voltage ride through in [27]. It is worth noting that although the occurrence time of irradiance variation and grid faults is set at $t = 1$ s and $t = 2$ s, the irradiance disturbance and the grid faults are separately applied in case studies, they do not occur at the same time.

Simulation results including power curve, d-q axis currents of PCC and the dc-link voltages of each PV unit are presented in case studies to verify the consistency between the aggregated model and the detailed model.

B. CASE 1: THE AGGREGATION MODEL OF MULTI-PARALLEL IDENTICAL PV UNITS WITH THE SAME IRRADIANCE INPUT

In this case, ten parallel identical PV units are aggregated into a separate PV system, which has the same parameters and structures. The power-stage and control parameters of identical PV units are listed in TABLE 1.

TABLE 1. Parameters of identical PV units and aggregated PV system.

Parameters	P	N_p	C_{PV}	L	C_{dc}	L_f	C_f	S_t
I-th (I=1-10) PV unit	0.3 MW	280	1000 μF	0.1 mH	10 mF	0.62 mH	20 μF	0.4 MVA
Equivalent value	3 MW	280 0	10 mF	0.01m H	100 mF	0.062 mH	200μ F	4 MVA

Parameters	k_{po}	k_{io}	k_{pdc}	k_{idc}	k_{pd}	k_{id}	k_{pq}	k_{iq}
I-th (I=1-10) PV unit	3000	30000	0.64	80	0.45	70	0.45	70
Equivalent value	3000	30000	6.4	800	0.45	70	0.45	70

	Computational Time
Detailed model	2843s
Aggregated model	46s

It can be noted from TABLE 1 that the inductance and resistance of aggregated model are reduced while the capacitance increases. Furthermore, it can be observed from TABLE 1 that the computational time of the aggregated model is far less than the time consumed by the detailed model. It is verified that the aggregated model can effectively reduce the computational burden caused by the detailed model. In addition, irradiance disturbance and grid faults transient are separately applied in the detailed model and the aggregated model to

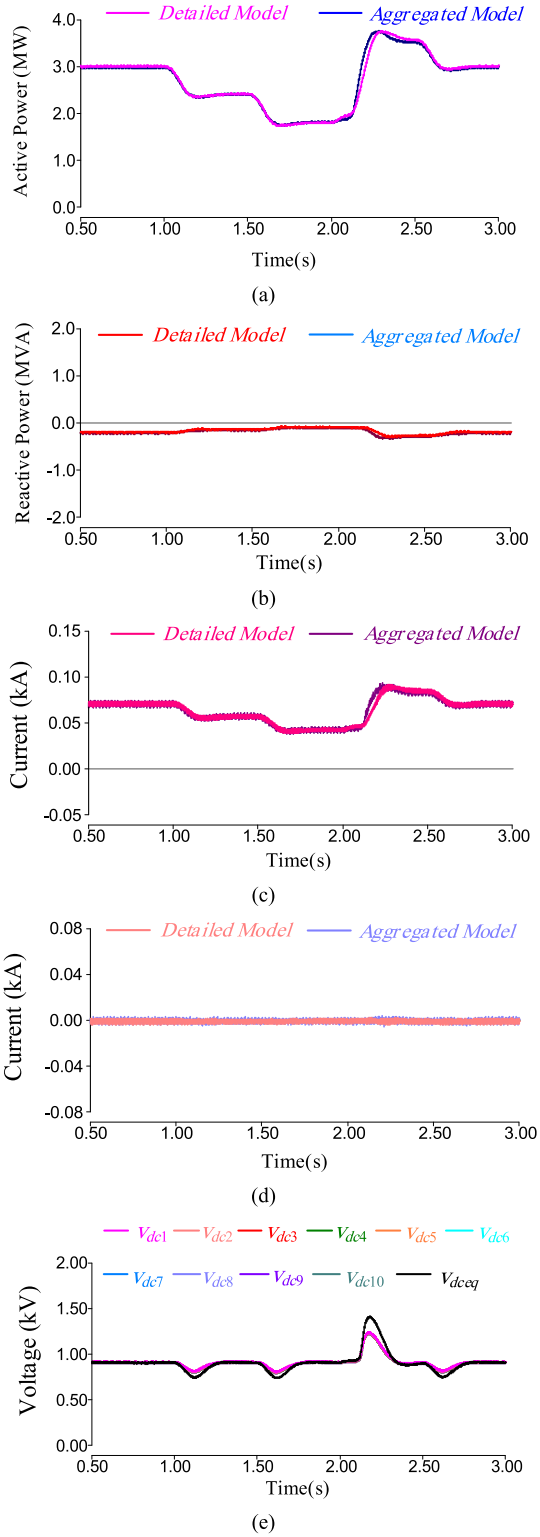

FIGURE 6. Simulation results of the detailed model and aggregated model under the condition of irradiance disturbance without grid faults in Case 1. (a) active power curve; (b) reactive power curve; (c) *d*-axis current; (d) *q*-axis current; (e) dc-link voltages of front-end circuit.

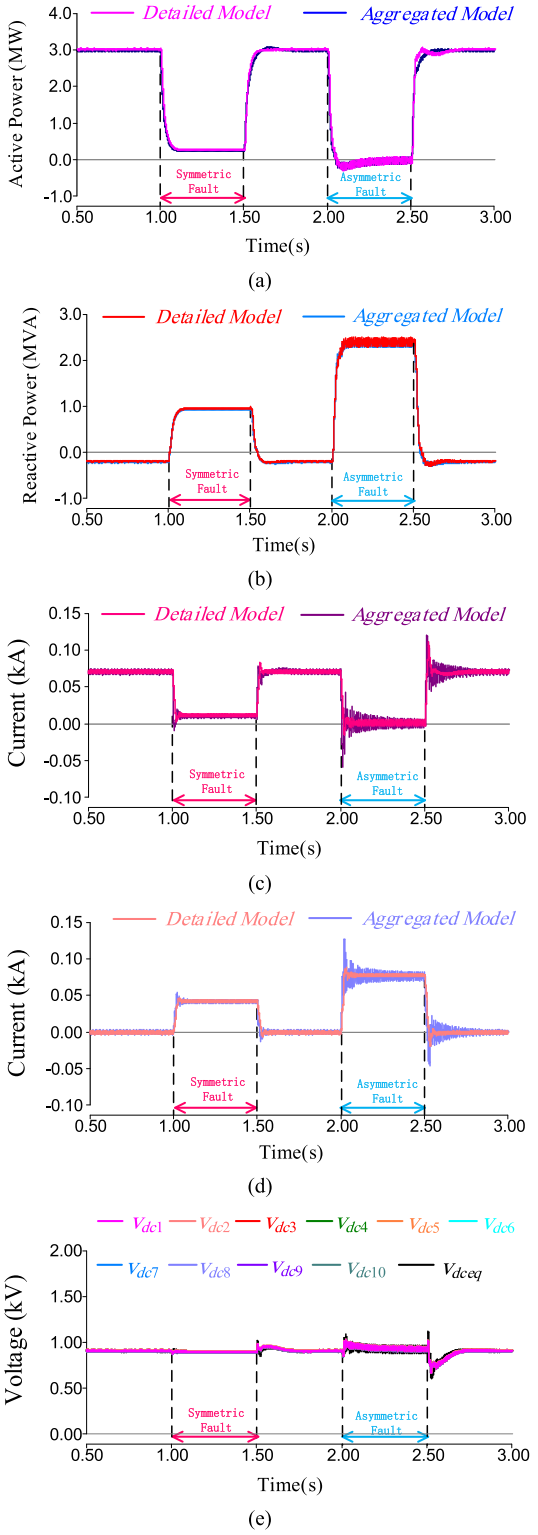

FIGURE 7. Simulation results of the detailed model and aggregated model under the condition of grid faults without irradiance disturbance in Case 1. (a) active power curve; (b) reactive power curve; (c) *d*-axis current; (d) *q*-axis current; (e) dc-link voltages of front-end circuit.

verify the effectiveness of the aggregation method. The simulation results under the condition of irradiance disturbance without grid faults is shown in Fig. 6, and the simulation results under grid faults transient without irradiance disturbance is depicted in Fig. 7.

It can be observed that the PCC power curves of aggregated model are consistent with the detailed model, as shown in Fig. 6(a)-(b). The active power and reactive power both vary with the changes of irradiance. The active power varies with the maximum 3.5 MW at 1200 W/m^2 input irradiance and the minimum 1.8 MW when the input irradiance is 600 W/m^2. However, the reactive power changes slightly since it is not determined by input irradiance. In the steady state of the standard condition with 1000 W/m^2 input irradiance, the active power is 3 MW, and the reactive power is −233 kVA, which is consumed by the transformers connected to the PCC. Fig. 6(c)-(d) depict the d-q axis currents of the detailed model and the aggregated model. It is observed that the dynamic response at $t = 2$ s shows a little discrepancy with the detailed model, which is caused by the large irradiance variation from 600 W/m^2 to 1200 W/m^2. Yet the steady state characteristics and most dynamic response of the aggregated model are consistent with the detailed model.

As shown in Fig. 6(e), the dc-link voltages of ten-parallel PV units in the detailed model are overlapped because of identical PV units. The v_{dceq} represents the dc-link voltage of the aggregated model, which shows the same steady state characteristics with the detailed model. The parallel number of PV arrays in aggregated model is the sum of the parallel numbers of ten-parallel PV units in detailed model. Although with the same irradiance condition, the power generated by one PV unit is much less than the power generated by the aggregated model. Therefore, the small response errors in regulating process exist between the aggregated model and the detailed model. However, the steady-state characteristic of aggregated model is consistent with the detailed model. It is verified that the aggregated model can reflect the steady state and dynamic response of the detailed model from both front-end and PCC characteristics.

From Fig. 7(a)-(b), the power curves of the aggregated model show the accordant steady state characteristic with the detailed model. Except for minor discrepancies at the asymmetric fault clearance time as shown in Fig. 7(a), the dynamic characteristics of the aggregated model are consistent with the detailed model. As shown in Fig. 7(c)-(d), the current curves have double-line-frequency fluctuations from $t = 2$s to $t = 2.5$ s due to unbalanced grid fault. Moreover, since the equivalent inductance in aggregated model is less than the inductance in the detailed model, the aggregated model has larger current ripple than the detailed model. However, ignoring the current ripple caused by low inductance, the most steady-state and dynamic responses of the aggregated model are consistent with the detailed model. In addition. the dc-link voltage of the aggregated model is also consistent with the dc-link voltages of the detailed model, which is overlapping as shown in Fig. 7 (e). It demonstrates that the aggregation methods can ensure that the aggregated model has the same steady state characteristic and dynamic response than the detailed model.

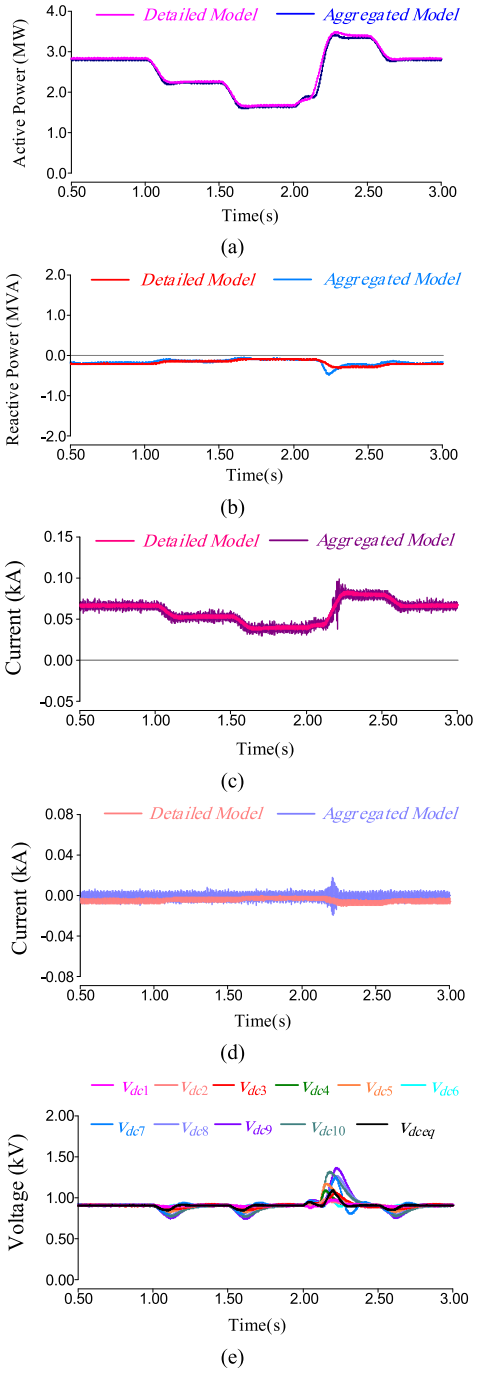

FIGURE 8. Simulation results of the detailed model and aggregated model under the condition of irradiance disturbance without grid faults in Case 2. (a) active power curve; (b) reactive power curve; (c) d-axis current; (d) q-axis current; (e) dc-link voltages of front-end circuit.

C. CASE 2: THE AGGREGATION MODEL OF MULTI-PARALLEL DIFFERENT PV UNITS WITH THE SAME IRRADIANCE INPUT

In this case, ten-parallel PV units with different parameters and power ratings are aggregated to a common PV system. It is worth noting that the ten-parallel different PV units are built in PSCAD/EMTDC platform with the constraint that the maximum variation ratio of the grid-connected line currents

TABLE 2. Parameters of detailed PV units and aggregated PV system.

Parameters	P(kW)	N_p	C_{PV} (μF)	L(mH)	C_{dc} (mF)	L_f (mH)	C_f (μF)	S_t (MVA)
1st-PV unit	43	80	400	0.01	5	0.12	5	0.2
2nd- PV unit	43	80	480	0.02	5.8	0.16	8	0.2
3rd- PV unit	185	180	643	0.035	6.5	0.23	10	0.4
4-th PV unit	185	180	500	0.045	7.05	0.31	12	0.4
5-th PV unit	300	280	552	0.055	7.4	0.42	15	0.4
6-th PV unit	300	280	600	0.058	7.85	0.49	18	0.4
7-th PV unit	400	380	680	0.078	8.06	0.53	20	0.5
8-th PV unit	400	380	770	0.1	8.57	0.38	16	0.5
9-th PV unit	500	460	808	0.086	8.43	0.58	25	0.6
10-th PV unit	500	460	1200	0.18	10	0.62	22	0.6
equivalent value	2856	2760	6633	0.00362	74.66	0.02904	149	4.2

Parameters	k_{po}	k_{io}	k_{pdc}	k_{idc}	k_{pd}	k_{id}	k_{pq}	k_{iq}
1st-PV unit	3000	30000	0.5	76	0.2	20	0.2	20
2nd- PV unit	3000	30000	0.74	100	0.32	64	0.32	64
3rd- PV unit	3000	30000	0.45	70	0.26	7	0.26	7
4-th PV unit	3000	30000	0.7	89	0.23	69	0.23	69
5-th PV unit	3000	30000	0.66	95	0.37	38	0.37	38
6-th PV unit	3000	30000	0.88	107	0.34	115	0.34	115
7-th PV unit	3000	30000	0.38	114	0.32	60	0.32	60
8-th PV unit	3000	30000	0.55	118	0.38	50	0.38	50
9-th PV unit	3000	30000	0.64	126	0.4	75	0.4	75
10-th PV unit	3000	30000	0.72	138	0.35	70	0.35	70
equivalent value	3000	30000	6.22	1033	0.342	62.85	0.342	62.85

	Computational Time
Detailed model	3018s
Aggregated model	42s

of different PV units during a disturbance (symmetric grid fault) is less than the coherency tolerance $\varepsilon = 0.8$, which is a modest tolerance analyzed in [7]. Therefore, those parallel PV units are coherent and they have little difference on the dynamic characteristics. The different parameter settings of multi-parallel units in the detailed model and the calculated equivalent parameters of the aggregated model are listed in TABLE 2.

The same conclusion can be summarized from TABLE 2 that the aggregated inductance decreases and the aggregated capacitance increases. Simultaneously, it is observed that the computational time of the aggregated model is much less than the time consumed by the detailed model. It is suggested that the aggregated model delivers similar dynamic responses to the detailed model in a strongly reduced amount of time. Moreover, irradiance disturbance and grid faults transient are separately applied in the detailed model and the aggregated model to verify the effectiveness of the aggregation method. The simulation results under the condition of irradiance disturbance without grid faults and the simulation results under grid faults transient without irradiance disturbance are shown in Fig. 8 and Fig. 9, respectively.

As shown in Fig. 8(a)-(b), when the input irradiance varies from 600 W/m^2 to 1200 W/m^2, the dynamic response of the aggregated model has a little discrepancy with the detailed model. However, the steady state characteristic and most dynamic responses of power curves of the aggregated model are consistent with the detailed model. Furthermore, the d-q axis currents of the aggregated model have the accordant steady state and dynamic response with the detailed model as shown in Fig. 8(c)-(d), which verifies the effectiveness of

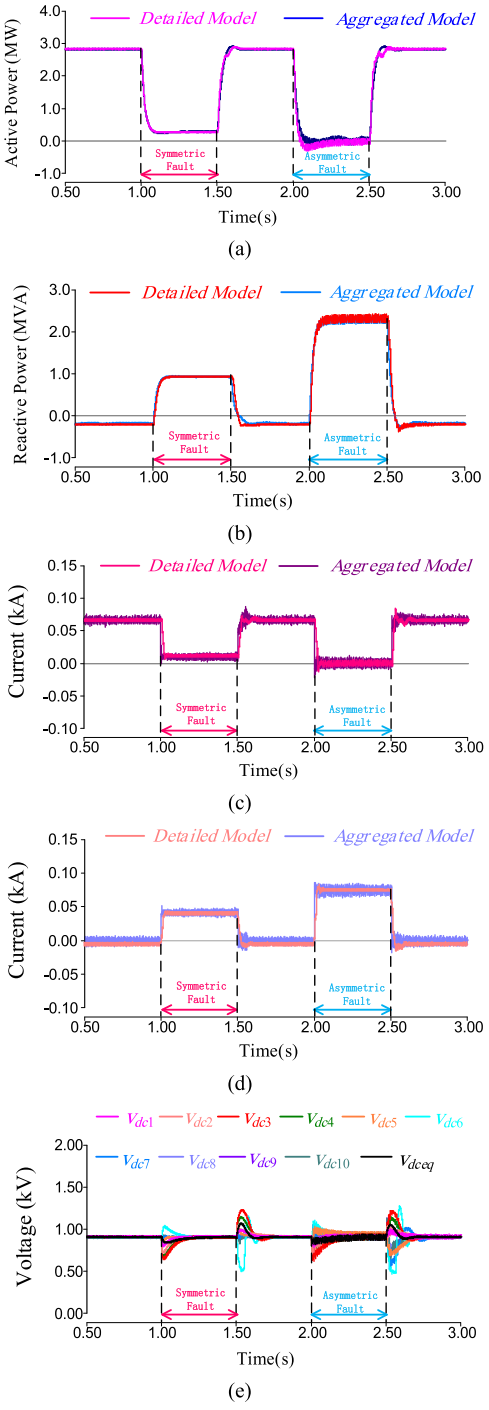

FIGURE 9. Simulation results of detailed model and aggregated model under the condition of grid faults without irradiance disturbance in Case 2. (a) active power curve; (b) reactive power curve; (c) *d*-axis current; (d) *q*-axis current; (e) dc-link voltages of front-end circuit.

the parameter calculation method of the aggregated model. Fig. 8(e) depicts that the dc-link voltages of the aggregated model and the detailed model. It can be noted that although that ten different and paralleled PV units have different dynamic response, the steady state and dynamic process of the detailed model can be basically reflected by v_{dceq} of the

TABLE 3. Irradiance intensity and power of parallel PV units in the detailed model.

	1-st	2-nd	3-rd	4-th	5-th	6-th	7-th	8-th	9-th	10-th
G_l (W/m^2)	550	600	650	700	750	800	850	900	950	1000
P_l (kW)	19	22	112	126	221	236	344	366	462	490

aggregated model, and it demonstrates the model consistency from the aspect of front-end circuit.

It can be observed from Fig. 9(a)-(b) that the output power of the aggregated model is matching with the detailed model in the steady state. The dynamic characteristic of the aggregated model is consistent with the detailed model, and minor discrepancies only exist at the clearance time of unbalanced grid fault as shown in Fig. 9(a). Moreover, the steady-state and dynamic characteristic of d-q axis currents of the aggregated model are consistent with the detailed model as shown in Fig. 9(c)-(d), which confirms the effectiveness of the aggregated model. Fig. 9(e) shows the dc-link voltages of the detailed model. They have the different regulating process at the occurrence and clearance of grid faults, but the dynamic characteristics of the detailed model can be basically reflected by the voltage v_{dceq} of the aggregated model, and two models have uniform steady state characteristic. It is concluded that the overall characteristic of the detailed model can be analyzed by using the aggregated model.

D. CASE 3: THE AGGREGATION MODEL OF MULTI-PARALLEL DIFFERENT PV UNITS WITH DIVERSE IRRADIANCE INPUT

In order to approach the actual situation in real application, the aggregation model of ten-parallel different PV units with different parameters and power ratings under the condition of diverse irradiance input is established in this case. The ten-parallel PV units have the same power-stage and control parameters than in Case 2, as listed in TABLE 2. It is worth noting that due to the diverse irradiance condition, although some units have the same series and parallel numbers in PV arrays, the power of each PV unit is different. Due to the same power between the aggregated model and the detailed model, the equivalent irradiance of the aggregated model can be obtained by the capacity weighting method. Hence, the equivalent irradiance intensity G_{eq} is presented as:

$$G_{eq} = \frac{\sum_{l=1}^{n} G_l A_l}{A_{eq}} = \frac{\sum_{l=1}^{n} G_l N_{sl} N_{pl}}{N_{seq} N_{peq}} \tag{45}$$

where A_{eq} is irradiated area of PV array in the aggregated model, and the G_l and A_l represent the irradiance intensity and irradiated area of PV array in l-th PV unit, respectively.

The irradiance input conditions and the power of each PV unit are given in TABLE 3. In addition, according to (45), the equivalent irradiance intensity in the aggregated model is calculated as 844.5262 W/m^2.

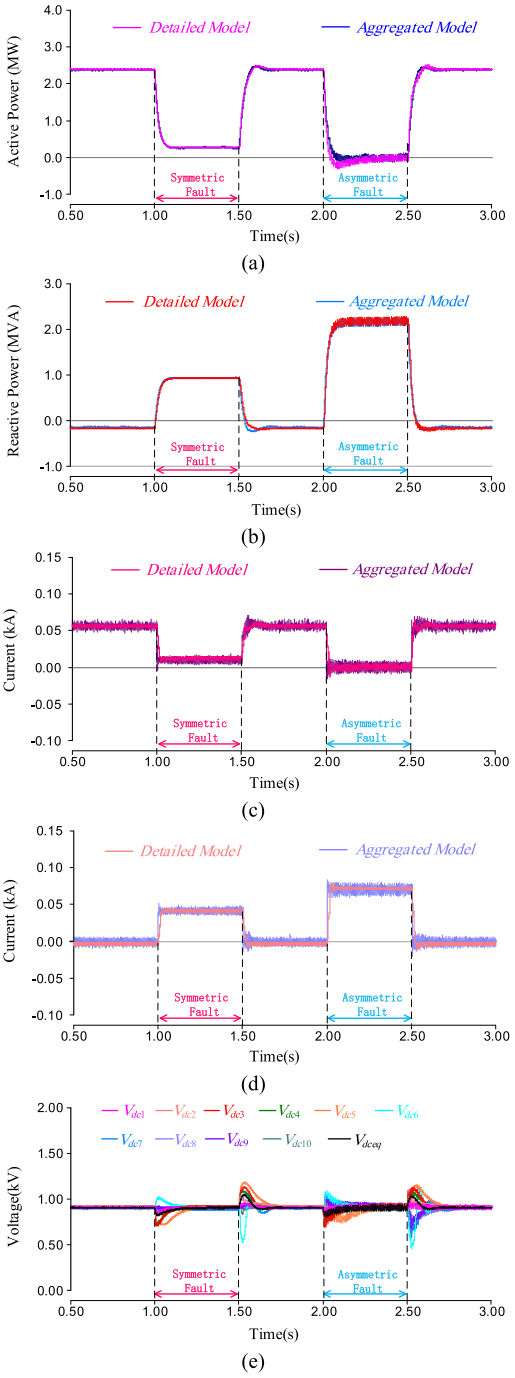

FIGURE 10. Simulation results of detailed model and aggregated model under the condition of grid faults in Case 3. (a) active power curve; (b) reactive power curve; (c) d-axis current; (d) q-axis current; (e) dc-link voltages of front-end circuit.

The simulation results of the detailed model and the aggregated model under the condition of continuous grid faults are depicted in the Fig. 10.

As shown in Fig. 10(a)-(b), the power curves of the aggregated model are consistent with the curves of the detailed model. Little discrepancy exists at $t = 2$ s in the active power curves, but the whole dynamic response of the aggregated

model is consistent with the detailed model. In addition, it can be observed from Fig. 10(c)-(d) that the steady state and dynamic response of d-q axis currents at PCC of the aggregated model is consistent with the detailed model. Fig. 10(e) shows the dc-link voltages of the detailed model. They have the different dynamic response at the occurrence and clearance of grid faults, but the steady state and dynamic characteristics can be basically reflected by the dc-link voltage v_{dceq} of the aggregated model. It is confirmed that when the parallel PV units have diverse irradiance condition, the overall characteristics of the detailed model can also be analyzed by using the aggregated model.

E. CASE 4: THE AGGREGATION MODEL OF MULTI-PARALLEL DIFFERENT PV UNITS UNDER THE CONDITION OF WEAK GRID

In order to confirm the impact of external grid strength on the aggregation method, the aggregated model under weak grid condition is built in this case. The grid strength is represented by the short circuit ration (SCR) and it can be written as [28]:

$$SCR = \frac{v_{pcc}^2}{|Z_g| P_{pcc}} \tag{46}$$

where Z_g is the grid impedance and P_{pcc} represents the power injected into PCC. Moreover, when a SCR is calculated below 3, the grid can be regarded as weak grid [29].

The impedance of grid is chosen as $Z_g = 60 + 0.425s$, and SCR is calculated as 2.98. The same external grid impedance Z_g is applied in both the detailed model and the aggregated model in this case, and the parameters of the detailed model and the aggregated model are also the same as in Case 2. The simulation results of the aggregated model and the detailed model under the condition of grid faults with weak grid circumstance are shown in Fig. 11.

Since there are 10-parallel PV units in the detailed model, the equivalent grid impedance of each PV unit is 10-times the original grid impedance [19]. The stability of the detailed model is deteriorated much than the aggregated model by the larger equivalent grid impedance. Therefore, it can be observed from Fig. 11(a)-(b) that the PCC power curves of the detailed model have a longer and steeper dynamic response at the occurrence and clearance of grid faults. Furthermore, the consistency of dynamic response between the aggregated model and the detailed model is deteriorated by the stability issues. In addition, the same phenomenon can be found in current curves, as shown in Fig. 11(c)-(d). Moreover, the consistency of dc-link voltage between the aggregated model and the detailed model also deteriorates with a weak grid circumstance, as shown in Fig. 11(e). However, if considering the stability issues caused by weak grid, it is rational to deem that the aggregated model is also valid, since the steady-state and dynamic characteristic of the detailed model can be basically reflected by the aggregated model, as shown in Fig. 11. In addition, it demonstrates that, when the external grid strength is weakened, the stability issues need to be considered in the aggregation method in the further work, but which is not the main scope of this paper.

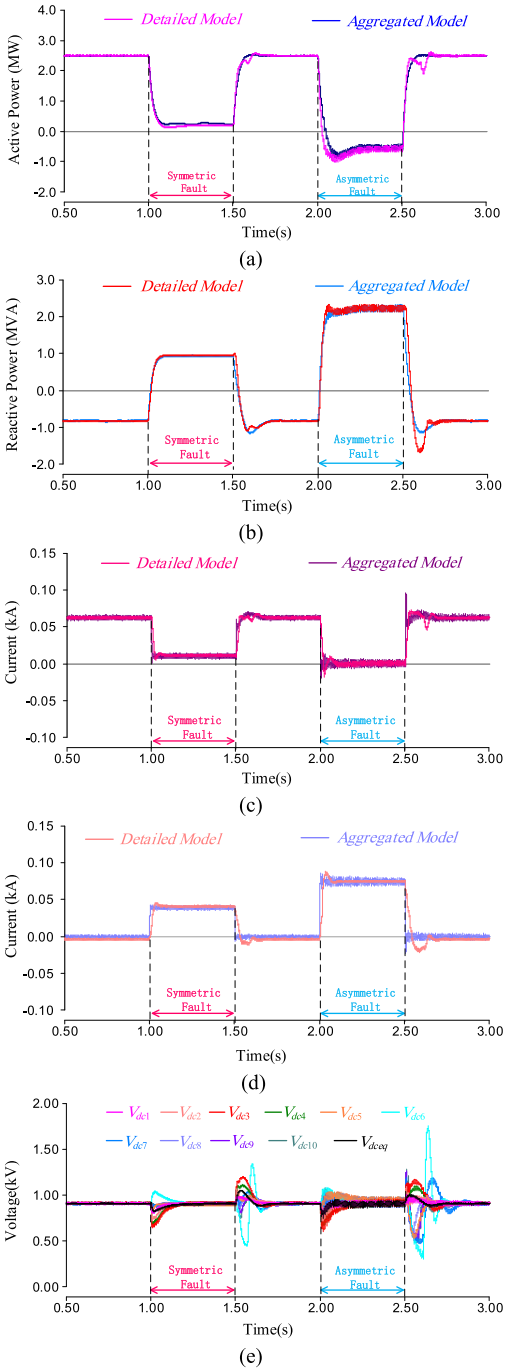

FIGURE 11. Simulation results of detailed model and aggregated model under the condition of grid faults with weak grid circumstance. (a) active power curve; (b) reactive power curve; (c) d-axis current; (d) q-axis current; (e) dc-link voltages of front-end circuit.

V. CONCLUSION

A structure-preserving aggregation method of large-scale multi-parallel PV system has been proposed in this paper, which can well capture the steady state and dynamic characteristics of the detailed model. The complete dynamic

modeling of two-stage PV system is derived including the PV arrays, front-end Boost converter, and rear-end grid-connected inverter, which is the basis of the aggregation method. The energy relationship in two-stage PV system is analyzed based on the Hamilton-action principle, hence, the relationship between the state variables of two coherent PV systems can be deduced. Then, the equivalent power-stage and control parameters are scaled by comparing the dynamic equations of the detailed model with the aggregated model.

Four different case studies have been established to verify the effectiveness of the proposed aggregated model, which includes the aggregation of ten-parallel identical PV units and ten-parallel different PV units both with the same irradiance condition, and the aggregation of different PV units under diverse irradiance and weak grid scenarios. It is confirmed that the proposed method is suitable for both the aggregation of identical and different multi-parallel PV units, and it can be applied in different scenarios. In addition, the consistency between the dynamic aggregated model and the detailed model is confirmed by the simulation results from PSCAD/EMTDC platform under the condition of different disturbances like irradiance variation, and continuous symmetric and asymmetric grid faults. Therefore, the aggregated model can be employed to accurately estimate the dynamics of the large-scale PV system in practical applications.

REFERENCES

[1] M. El-Shimy, A. Sharaf, H. Khairy, and G. Hashem, "Reduced-order modelling of solar-PV generators for small-signal stability assessment of power systems and estimation of maximum penetration levels," *IET Gener. Transm. Distrib.*, vol. 12, no. 8, pp. 1838–1847, Apr. 2018.

[2] Y. Xia, M. Yu, X. Wang, and W. Wei, "Describing function method based power oscillation analysis of LCL-filtered single-stage PV generators connected to weak grid," *IEEE Trans. Power Electron.*, vol. 34, no. 9, pp. 8724–8738, Sep. 2019.

[3] Y. Xia, Y. Peng, P. Yang, Y. Li, and W. Wei, "Different influence of grid impedance on low- and high-frequency stability of PV generators," *IEEE Trans. Ind. Electron.*, vol. 66, no. 11, pp. 8498–8508, Nov. 2019.

[4] A. Sangwongwanich, Y. Yang, and F. Blaabjerg, "A sensorless power reserve control strategy for two-stage grid-connected PV systems," *IEEE Trans. Power Electron.*, vol. 32, no. 11, pp. 8559–8569, Nov. 2017.

[5] H. D. Tafti, A. Sangwongwanich, Y. Yang, J. Pou, G. Konstantinou, and F. Blaabjerg, "An adaptive control scheme for flexible power point tracking in photovoltaic systems," *IEEE Trans. Power Electron.*, vol. 34, no. 6, pp. 5451–5463, Jun. 2019.

[6] E. Afshari, G. R. Moradi, R. Rahimi, B. Farhangi, Y. Yang, F. Blaabjerg, and S. Farhangi, "Control strategy for three-phase grid-connected PV inverters enabling current limitation under unbalanced faults," *IEEE Trans. Ind. Electron.*, vol. 64, no. 11, pp. 8908–8918, Nov. 2017.

[7] X. Zha, S. Liao, M. Huang, Z. Yang, and J. Sun, "Dynamic aggregation modeling of grid-connected inverters using hamilton's-action-based coherent equivalence," *IEEE Trans. Ind. Electron.*, vol. 66, no. 8, pp. 6437–6448, Aug. 2019.

[8] S. Liao, X. Zha, X. Li, M. Huang, J. Sun, J. Pan, and J. M. Guerrero, "A novel dynamic aggregation modeling method of grid-connected inverters: Application in small-signal analysis," *IEEE Trans. Sustain. Energy*, vol. 10, no. 3, pp. 1554–1564, Jul. 2019.

[9] X. Du, Y. Zhang, Q. Li, Y. Xiong, X. Yu, and X. Zhang, "New theory of extended coherency for power system based on method of coherency in differential geometry," in *Proc. Asia–Pacific Power Energy Eng. Conf.*, Wuhan, China, 2011, pp. 1–6.

[10] C. Li, J. Xu, and C. Zhao, "A coherency-based equivalence method for MMC inverters using virtual synchronous generator control," *IEEE Trans. Power Del.*, vol. 31, no. 3, pp. 1369–1378, Jun. 2016.

[11] P. J. Hart, R. H. Lasseter, and T. M. Jahns, "Coherency identification and aggregation in grid-forming droop-controlled inverter networks," *IEEE Trans. Ind. Appl.*, vol. 55, no. 3, pp. 2219–2231, May 2019.

[12] V. Purba, B. B. Johnson, M. Rodriguez, S. Jafarpour, F. Bullo, and S. Dhople, "Reduced-order aggregate model for parallel-connected single-phase inverters," *IEEE Trans. Energy Convers.*, vol. 34, no. 2, pp. 824–837, Jun. 2019.

[13] A. Samadi, L. Söder, E. Shayesteh, and R. Eriksson, "Static equivalent of distribution grids with high penetration of PV systems," *IEEE Trans. Smart Grid*, vol. 6, no. 4, pp. 1763–1774, Jul. 2015.

[14] Z. Shuai, Y. Peng, X. Liu, Z. Li, J. M. Guerrero, and Z. J. Shen, "Dynamic equivalent modeling for multi-microgrid based on structure preservation method," *IEEE Trans. Smart Grid*, vol. 10, no. 4, pp. 3929–3942, Jul. 2019.

[15] Z. Yuan, Z. Du, C. Li, and T. An, "Dynamic equivalent model of VSC based on singular perturbation," *IET Gener. Transmiss. Distrib.*, vol. 10, no. 14, pp. 3413–3422, Oct. 2016.

[16] A. Bonfiglio, F. Delfino, M. Invernizzi, R. Procopio, and P. Serra, "Criteria for the equivalent modeling of large photovoltaic power plants," in *Proc. IEEE PES General Meeting. Conf. Expo.*, National Harbor, MD, USA, Jul. 2014, pp. 1–5.

[17] H. Meng, X. Ye, M. Yang, X. Song, Z. Su, W. Liu, L. Luo, and H. Zhao, "Equivalent modeling and simulation for PV system on dynamic clustering equivalent strategy," in *Proc. IEEE IECON*, Beijing, China, Oct./Nov. 2017, pp. 5779–5784.

[18] D. Remon, A. M. Cantarellars, and P. Rodriguez, "Equivalent model of large-scale synchronous photovoltaic power plants," *IEEE Trans. Ind. Appl.*, vol. 52, no. 6, pp. 5029–5040, Nov. 2016.

[19] J. L. Agorreta, M. Borrega, J. López, and L. Marroyo, "Modeling and control of N-paralleled grid-connected inverters with LCL filter coupled due to grid impedance in PV plants," *IEEE Trans. Power Electron.*, vol. 26, no. 3, pp. 770–785, Nov. 2011.

[20] Z. Moradi-Shahrbabak and A. Tabesh, "Effects of front-end converter and DC-link of a utility-scale PV energy system on dynamic stability of a power system," *IEEE Trans. Ind. Electron.*, vol. 65, no. 1, pp. 403–411, Jan. 2018.

[21] M. A. G. de Brito, L. Galotto, L. P. Sampaio, G. E. de Azevedo e Melo, and C. A. Canesin, "Evaluation of the main MPPT techniques for photovoltaic applications," *IEEE Trans. Ind. Electron.*, vol. 60, no. 3, pp. 1156–1167, Mar. 2013.

[22] N. Femia, G. Petrone, G. Spagnuolo, and M. Vitelli, "Optimization of perturb and observe maximum power point tracking method," *IEEE Trans. Power Electron.*, vol. 20, no. 4, pp. 963–973, Jul. 2005.

[23] A. Yazdani, A. R. Di Fazio, H. Ghoddami, M. Russo, M. Kazerani, J. Jatskevich, K. Strunz, S. Leva, and J. A. Martinez, "Modeling guidelines and a benchmark for power system simulation studies of three-phase single-stage photovoltaic systems," *IEEE Trans. Power Del.*, vol. 26, no. 2, pp. 1247–1264, Apr. 2011.

[24] T. Esram and P. L. Chapman, "Comparison of photovoltaic array maximum power point tracking techniques," *IEEE Trans. Energy Convers.*, vol. 22, no. 2, pp. 439–449, Jun. 2007.

[25] M. Fazeli, J. B. Ekanayake, P. M. Holland, and P. Igic, "Exploiting PV inverters to support local voltage—A small-signal model," *IEEE Trans. Energy Convers.*, vol. 29, no. 2, pp. 453–462, Jun. 2014.

[26] Y. Han, H. Chen, Z. Li, P. Yang, L. Xu, and J. M. Guerrero, "Stability analysis for the grid-connected single-phase asymmetrical cascaded multilevel inverter with SRF-PI current control under weak grid conditions," *IEEE Trans. Power Electron.*, vol. 34, no. 3, pp. 2052–2069, Mar. 2019.

[27] X. Lin, Y. Han, P. Yang, C. Wang, and J. Xiong, "Low-voltage ride-through techniques for two-stage photovoltaic system under unbalanced grid voltage sag conditions," in *Proc. IEEE 4th Southern Power Electron. Conf. (SPEC)*, Singapore, Dec. 2018, pp. 1–8.

[28] N. N. K, S. S, and L. Umanand, "Stability analysis of phase locked loop controllers for grid tied inverters in weak microgrids," in *Proc. IEEE Int. Conf. Power Electron., Drives Energy Syst. (PEDES)*, Chennai, India, Dec. 2018, pp. 1–5.

[29] *IEEE Guide for Planning DC Links Terminating at AC Locations Having Low Short-Circuit Capacities*, IEEE Standards 1204-1997, Jan. 1997, pp. 1–216.

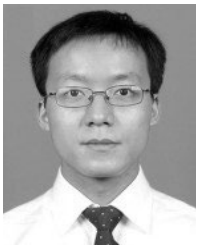

YANG HAN (Senior Member, IEEE) received the Ph.D. degree in electrical engineering from Shanghai Jiao Tong University (SJTU), Shanghai, China, in 2010.

In 2010, he joined the Department of Power Electronics, School of Mechatronics Engineering, University of Electronic Science and Technology of China (UESTC), Chengdu, China, where he has been an Associate Professor, since 2013. He is currently with the Department of Electrical Engineering, School of Mechanical and Electrical Engineering, UESTC. From March 2014 to March 2015, he was a Visiting Scholar with the Department of Energy Technology, Aalborg University, Aalborg, Denmark. He has authored more than 20 ISI-indexed international journal articles, including three ESI highly cited article, one ESI hot article, and one book chapter in the area of power electronics, power quality conditioners, and smart grid. He holds 25 issued and nine pending patents. His research interests include the ac/dc microgrids, active distribution networks, power quality, grid-connected converters for renewable energy systems, active power filters, multilevel converters, and static synchronous compensators (STATCOMs).

Dr. Han was a recipient of the Academic Talent Award by UESTC, in 2017, and Baekhyun Award by the Korean Institute of Power Electronics, in 2016. He was also a recipient of the Best Paper Awards from the 34th Annual Conference on Power System and Automation of Chinese Universities, in 2018, the Joint Conference of Sichuan Power Supply Society and Chongqing Power Supply Society, in 2018, the 6th Asia International Symposium on Mechatronics, in 2017, the 5th National Conference on Power Quality, in 2017, the Annual Conference of HVDC and Power Electronics Committee of Chinese Society of Electrical Engineers, in 2013, and the 4th International Conference on Power Quality, in 2008, China. He was a Session Chair for Power Quality and Premium Power Supply Session in 35th Annual Conference on Power System and Automation of Chinese Universities, Chengdu, China, in 2019, for Emerging Technologies and End-user Systems, Grid Operation and Management, and Power Electronics, Control and Protection Systems for Smart Grids Sessions in IEEE PES Innovative Smart Grid Technologies Asia (ISGT Asia 2019), Chengdu, China, in 2019, for Microgrid and Distributed Generation Session in the Symposium on Power Electronics and Electrical Drives (SPEED), Xi'an, China, in 2019, for Microgrid Optimization and Scheduling Session in the 2nd International Conference on Power and Renewable Energy, Chengdu, China, in 2017, for Power Quality Mitigation and Application Session in the 5th National Conference on Power Quality, Xi'an, China, in 2017, and for AC/DC, DC/AC Power Converter Session in the 2016 IPEMC ECCE-Asia, Hefei, China. He is an Associate Editor for IEEE Access and the *Journal of Power Electronics* (JPE).

XIANGYANG LIN received the B.S. degree in electrical engineering and automation from the University of Electronic Science and Technology of China (UESTC), Chengdu, China, in 2018, where he is currently pursuing the M.S. degree in power electronics and electric drives. His main research interests include stability analysis of inverters and modeling of the renewable-energy generation systems.

PING YANG received the B.S. degree in mechanical engineering from Shanghai Jiao Tong University (SJTU), Shanghai, China, in 1984, and the M.S. degree in mechanical engineering from Sichuan University, in 1987.

He was visiting Victory University, Australia, from July 2004 to August 2004, and a Visiting Scholar with the S. M. Wu Manufacturing Research Center, University of Michigan, Ann Arbor, USA, from August 2009 to February 2010, and was visiting the University of California at Irvine, Irvine, USA, from October 2012 to November 2012. He is currently a Full Professor with the School of Mechatronics Engineering, University of Electronic Science and Technology of China (UESTC), Chengdu, China. He is also the Dean of the School of Mechanical and Electrical Engineering, UESTC. He has authored more than 60 articles in various journals and international conferences, and several books on mechatronics and instrumentation. He received several provincial awards for his contribution in teaching and academic research. His research includes mechatronics engineering, electrical engineering and automation, computer-aided control and instrumentation, smart mechatronics, and detection and automation of mechanical equipment.

LIN XU received the Ph.D. degree in electrical engineering from Shanghai Jiao Tong University (SJTU), Shanghai, China, in 2011. She is currently a Senior Engineer with the Sichuan Electric Power Research Institute, State Grid Sichuan Electric Power Company, Chengdu, China. She has coauthored more than 20 journals and conference papers in the area of power electronics and power systems.

Her research interests include power quality, power system analysis, and real-time digital simulator (RTDS), and flexible Ac transmission systems (FACTS), such as STATCOMs and power quality conditioners (DVRs and APFs). She is an Active Reviewer of the IEEE Transactions on Industrial Electronics, the IEEE Transactions on Power Electronics, and *Electric Power Components and Systems*.

YAN XU (Senior Member, IEEE) received the B.E. and M.E degrees from the South China University of Technology, Guangzhou, China, in 2008 and 2011, respectively, and the Ph.D. degree from The University of Newcastle, Australia, in 2013. He held The University of Sydney Postdoctoral Fellowship in Australia. He is currently an Assistant Professor with the School of Electrical and Electronic Engineering, Nanyang Technological University, Singapore. His research interests include power system stability and control, microgrid, and data-analytics for smart grid applications. Dr. Xu is an Editor of the IEEE Transactions on Smart Grid, *CSEE Journal of Power and Energy Systems*, and an Associate Editor for *IET Generation, Transmission & Distribution*.

FREDE BLAABJERG (Fellow, IEEE) received the Ph.D. degree in electrical engineering with Aalborg University, in 1995. He became an Assistant Professor, in 1992, an Associate Professor, in 1996, and a Full Professor of power electronics and drives, in 1998. From 2017, he became a Villum Investigator. He was with ABB-Scandia, Randers, Denmark, from 1987 to 1988. He has published more than 600 journal articles in the fields of power electronics and its applications. He has coauthored four monographs and Editor of ten books in power electronics and its applications. His current research interests include power electronics and its applications such as in wind turbines, PV systems, reliability, harmonics and adjustable speed drives.

He has received 31 IEEE Prize Paper Awards, the IEEE PELS Distinguished Service Award, in 2009, the EPE-PEMC Council Award, in 2010, the IEEE William E. Newell Power Electronics Award 2014, the Villum Kann Rasmussen Research Award 2014, and the Global Energy Prize, in 2019. He received an *honoris causa* at University Politehnica Timisoara (UPT), Romania, and Tallinn Technical University (TTU), Estonia. He was the Editor-in-Chief of the IEEE Transactions on Power Electronics, from 2006 to 2012. He has been Distinguished Lecturer for the IEEE Power Electronics Society, from 2005 to 2007 and for the IEEE Industry Applications Society, from 2010 to 2011 and 2017 to 2018. From 2019 to 2020, he serves as the President for the IEEE Power Electronics Society. He is the Vice President of the Danish Academy of Technical Sciences too. He is nominated in 2014–2018 by Thomson Reuters to be between the most 250 cited researchers in Engineering in the world.